ELSEVIER

Physica C 292 (1997) 39–47

PHYSICA C

The azimuthal critical state of a superconducting hollow cylinder

E. Altshuler *, R. Mulet

Superconductivity Laboratory, IMRE-Physics Faculty, University of Havana, La Habana 10400, Cuba

Received 17 February 1997; revised 29 May 1997; accepted 18 July 1997

Abstract

We use the critical state model to calculate the flux profiles and magnetization curves for type II superconducting hollow cylinders of different wall thicknesses subject to an azimuthal magnetic field produced by a coaxially arranged current-carrying wire. We analyze the cases of field-independent and field-decaying critical current densities, and systematically compare the results with those expected for the "conventional" slab geometry using parameters typical of a high temperature ceramic superconductor. Some new features are observed for the hollow cylinder, such as the different shape and the asymmetry of the flux distribution profiles, as well as the strong increase of the full penetration field and the field at which the magnetization curves have maxima, with the wall thickness. In our opinion, this feature is the one that should be compared with the experiment in order to test our results. © 1997 Elsevier Science B.V.

Keywords: Type II superconductors; Magnetization; Pinning; Critical current density

1. Introduction

Although straight vortices are widely analyzed in the literature on type II superconductors, circular vortices (which can be visualized as doughnut shaped flux tubes containing one flux quantum) have been rarely studied. However, such vortices can be present when transport currents are applied [1], and are thought to have a relevant role in the flux dynamics of high temperature superconductors [2,3]. De Gennes, for example, refers to them briefly in Ref. [4], while Tinkham [1] proposes a simple model for describing the behavior of the circular vortices which appear in a pinning-free type II superconducting bulk cylinder supporting an axial current. More recently Kozlov and Samokhavalov [5–7], and Genenko [8] have approached the subject by performing the exact calculation of the flux structure associated to circular vortices in solid cylinders. A similar work has been carried out by us [9,10] for the case of a hollow cylinder exposed to an azimuthal magnetic field, in which the appearance of asymmetric Bean–Livingstone surface barriers is reported. Later on, surface barriers of circular vortices close to a flat surface have been treated by Samokhvalov [11]. The dynamics of helical vortices produced by the combination of axial transport currents and magnetic fields in a superconducting wire have been treated by Clem [12] and, more recently, by Shvarster et al. [13].

The case of circular vortices in type II superconductors with pinning is a more complicated subject, and exact analytical expressions for the flux and current distributions are extremely difficult to obtain. From the experimental point of view, the extensive work of LeBlanc and coworkers must be pointed out, particularly their study of the response of cylinders

* Corresponding author. E-mail: jea@infomed.sld.cu

PII S0921-4534(97)01628-6

submitted to superimposed azimuthal and axial magnetic fields both for conventional [14] and high temperature [15] type II superconductors. The calculation of the flux distribution for such systems can be performed with the help of the critical state model [16,17] originally conceived for straight vortices (i.e., only axial fields applied). This kind of approach has been explored theoretically by Koppe [18], and Pérez-González and Clem [19].

In this paper, we apply Bean's [16,17] and Kim's [20] critical state hypotheses to a type II superconducting hollow cylinder with pinning subject to an azimuthal magnetic field produced by a current-carrying coaxial wire. We calculate and plot, in both cases, the flux distribution due to the presence of circular vortices into the wall of the cylinder, the magnetization curves, and the dependence of the full penetration field (H^*) on the wall thickness. We bring detailed formulae for all these curves in the case of Bean's hypothesis, while numerical results are obtained under Kim's hypothesis. Interestingly, we observe nonlinear flux profiles for the Bean's model, clearly different from the slab geometry. The application of Kim's hypothesis, on the other hand, yields profiles with curvature opposite to the one corresponding to the conventional geometry. In both cases H^* shows a stronger increase with wall thickness as compared with the slab. In the case of Kim's hypothesis, the thickness dependence of the field at which magnetization maxima occur is also plotted, and shows a behavior analogous to the one of H^*.

2. Statement of the problem

As originally proposed in Ref. [16], when a finite sample of type II superconducting material is in the mixed state, the vortices are distributed throughout the sample in such a way that, in each pinning center, a vortex (or a vortex bundle) is in equilibrium due to the compensation of a Lorentz-like force and a pinning force. This state of the entire sample is called *critical*, and the resulting flux density distribution, $\boldsymbol{h}(\boldsymbol{r})$, can be obtained by solving the equation

$$\nabla \times \boldsymbol{h}(\boldsymbol{r}) = \pm \mu_0 \boldsymbol{J}_c(\boldsymbol{r}) \tag{1}$$

where $\boldsymbol{J}_c(\boldsymbol{r})$ is the local critical current density.

Consider the case of an infinite hollow cylinder

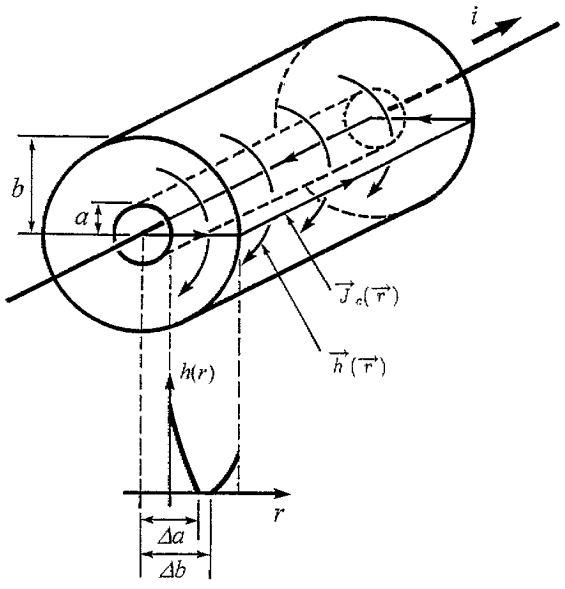

Fig. 1. Hollow cylinder plus current-carrying wire arrangement showing, in a simplified fashion, the current and magnetic flux distributions (above), and an azimuthal magnetic flux profile in the critical state (below).

with inner and outer radii a and b, respectively, made of a type II superconductor with pinning. An infinite coaxial wire carrying a current i exposes the cylinder to an azimuthal magnetic field. For this case, Eq. (1) can be written, in cylindrical coordinates, as:

$$\frac{\mathrm{d}}{\mathrm{d}r} h(r) + \frac{1}{r} h(r) = \pm \mu_0 J_c(r) \tag{2}$$

where r is the radius of the point for which h is calculated, and the "$\pm$" symbol expresses the directions of the current near the inner ($r = a$) and outer ($r = b$) surfaces of the hollow cylinder. The upper section of Fig. 1 shows (for the case of a non-infinite cylinder) a simplified example of how $\boldsymbol{h}(\boldsymbol{r})$ and the shielding currents, $\boldsymbol{J}_c(\boldsymbol{r})$, are arranged into the wall of the cylinder when the applied field is increasing.

The boundary conditions for $h(r)$ result from the application of Ampère's law over circular paths arranged with the same symmetry of the system. If it is applied over a path with radius $r_a < a$ very close to the inner surface of the cylinder, we get:

$$h(a) = \frac{\mu_0 i}{2\pi a} \tag{3}$$

whilst, if it is applied over a path with radius $r_b > b$ very close to the outer surface of the cylinder, taking into account that the shielding currents circulating parallel to the cylinder's axis compensate due to charge conservation, we get:

$$h(b) = \frac{\mu_0 i}{2\pi b} \tag{4}$$

In his original paper [16], Bean treated the special case when the critical current density is independent of the position (or, equivalently, of the local flux density). We will call this case *Bean's hypothesis*, which takes place when $J_c(r)$ is replaced by the constant value J_c in Eq. (2).

In Ref. [20], Kim et al. considered that the magnitude of the critical current density appearing in Eq. (1) dependent on the local field, as:

$$J_c(h) = \frac{J_c(0)}{1 + (h/h_0)} \tag{5}$$

where $J_c(0)$ is the critical current density at zero field, and h_0 is the magnetic induction at which the critical current of the superconductor decays to half of his zero-field value. We will call this *Kim's hypothesis*. Then, the equation analogous to Eq. (2) in this case turns to be:

$$\frac{\mathrm{d}}{\mathrm{d}r}h(r) + \frac{1}{r}h(r) = \frac{\pm\mu_0 J_c(0)}{1 + [h(r)/h_0]} \tag{6}$$

Here, boundary conditions Eqs. (3) and (4) are still valid.

3. Results and discussion

3.1. Bean's hypothesis

The general solution of Eq. (2) can be written as:

$$h(r) = \frac{C}{r} \pm \mu_0 J_c(0)\frac{r}{2} \tag{7}$$

where C is an integration constant which can be calculated when the boundary conditions Eqs. (3) and (4) are introduced. It is convenient to split the resulting expressions according to different stages of increasing or decreasing applied field (or, equivalently, applied current), as is usual in the literature [16,17]. In order to do that, it is convenient to define a few parameters. The lower part of Fig. 1 shows a hypothetical flux density versus r profile within the cylinder wall in current increase conditions (observe that we have represented asymmetric field penetrations from the inner and outer surfaces, which is coherent with our later results). This situation is similar to that represented in Fig. 2(a), in which Δa and Δb are defined as the radial distances from the inner wall to the points of maximum penetration of the field from $r = a$ and $r = b$, respectively. Fig. 2(b) shows a particular case in which the wire current has been increased to a value i^* called *full penetration current* for which the inner and outer flux density profiles just "meet" at some point at a

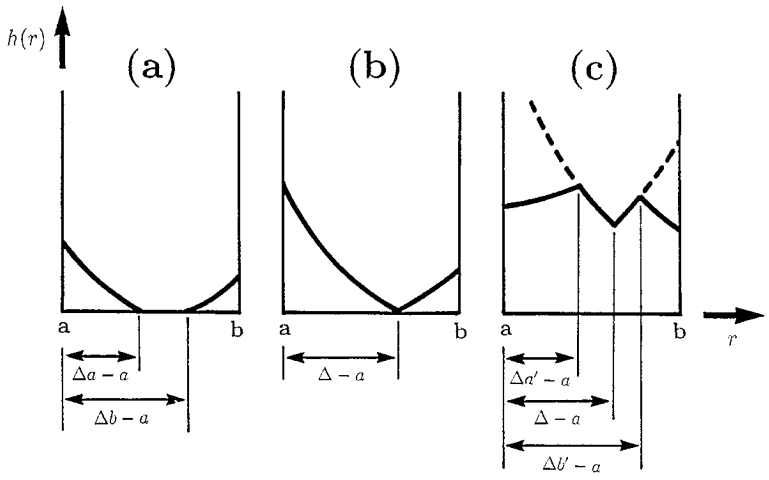

Fig. 2. Hypothetical flux distribution profiles in the critical state for increasing wire current before "full penetration" (a), increasing wire current in the case of "full penetration" (b), and decreasing wire current after having reached some maximum current (c).

distance Δ from the center. Fig. 2(c) shows the situation where, after a maximum current increase to i_{max} (whose profile has been represented in dotted lines), it has been decreased to some finite value. There, $\Delta a'$ and $\Delta b'$ are defined as the distances from the inner radius to the local flux density minima closer to $r = a$ and to $r = b$, respectively.

The results, are as follows.

Increasing field

(a) $i < i^*$

$$h(r) = \frac{\mu_0}{2}\left[-J_c r + \frac{1}{r}\left(\frac{i}{\pi} - J_c a^2\right)\right] \text{ if } a \le r \le \Delta a \tag{8}$$

$$h(r) = 0 \text{ if } \Delta a \le r \le \Delta b \tag{9}$$

$$h(r) = \frac{\mu_0}{2}\left[J_c r + \frac{1}{r}\left(\frac{i}{\pi} - J_c b^2\right)\right] \text{ if } \Delta b \le r \le b \tag{10}$$

(b) $i > i^*$

$$h(r) = \frac{\mu_0}{2}\left[-J_c r + \frac{1}{r}\left(\frac{i}{\pi} + J_c a^2\right)\right] \text{ if } a \le r \le \Delta \tag{11}$$

$$h(r) = \frac{\mu_0}{2}\left[J_c r + \frac{1}{r}\left(\frac{i}{\pi} - J_c b^2\right)\right] \text{ if } \Delta \le r \le b \tag{12}$$

where

$$i^* = \frac{\pi}{2} J_c (b^2 - a^2) \tag{13}$$

$$\Delta a = \sqrt{\frac{1}{J_c}\left(\frac{i}{\pi} + J_c a^2\right)} \tag{14}$$

$$\Delta b = \sqrt{\frac{1}{J_c}\left(-\frac{i}{\pi} + J_c b^2\right)} \tag{15}$$

and

$$\Delta = \sqrt{\frac{a^2 + b^2}{2}} \tag{16}$$

Decreasing field

Case (3) $2i^* < i_{max}$

(a) $i_{max} - 2i < i < 2i^*$

$$h(r) = \frac{\mu_0}{2}\left[J_c r + \frac{1}{r}\left(\frac{i}{\pi} - J_c a^2\right)\right] \text{ if } a \le r \le \Delta a' \tag{17}$$

$$h(r) = \frac{\mu_0}{2}\left[-J_c r + \frac{1}{r}\left(\frac{i_{max}}{\pi} + J_c a^2\right)\right] \text{ if } \Delta a' \le r \le \Delta \tag{18}$$

$$h(r) = \frac{\mu_0}{2}\left[J_c r + \frac{1}{r}\left(\frac{i_{max}}{\pi} - J_c b^2\right)\right] \text{ if } \Delta \le r \le \Delta b' \tag{19}$$

$$h(r) = \frac{\mu_0}{2}\left[-J_c r + \frac{1}{r}\left(\frac{i}{\pi} + J_c b^2\right)\right] \text{ if } \Delta b' \le r \le b \tag{20}$$

(b) $0 < i < i_{max} - 2i^*$

$$h(r) = \frac{\mu_0}{2}\left[J_c r + \frac{1}{r}\left(\frac{i}{\pi} - J_c a^2\right)\right] \text{ if } a \le r \le \Delta \tag{21}$$

$$h(r) = \frac{\mu_0}{2}\left[-J_c r + \frac{1}{r}\left(\frac{i}{\pi} + J_c b^2\right)\right] \text{ if } \Delta \le r \le b \tag{22}$$

Case (4) $i_{max} \le 2i^*$ (formulas (17)–(20) hold), where

$$\Delta a' = \sqrt{a^2 + \frac{i_{max} - i}{2\pi J_c}} \tag{23}$$

and

$$\Delta b' = \sqrt{b^2 - \frac{i_{max} - i}{2\pi J_c}} \tag{24}$$

Fig. 3 shows these results for the particular case of a 10 mm thick wall hollow cylinder compared to the analogous ones corresponding to a 10 mm thick infinite slab subject to a field parallel to its surfaces. A critical current density $J_c = 10^6$ A/m^2 ($= 10^2$ A/cm^2) was chosen in order to mimic the case of a typical high temperature $YBa_2Cu_3O_7$ superconducting ceramic [21]. In order to make the comparison easier, we plotted the external field of the cylinder at

$r = a$ in the y-axis, instead of i. Two differences between the flux distribution of the slab and that of the hollow cylinder are clearly observed. First, the cylinder shows nonlinear profiles both for increasing and for decreasing applied fields. Second, its profiles are not symmetric. It is worth noting that the cylinder "supports" relatively high fields at the inner wall without being completely penetrated (Fig. 3c); however, when high wire currents are applied, the shielding capacity tends to zero, and a nearly hyperbolic profile is obtained. It should be noticed that, contrary to the case of the slab, in the cylindrical geometry the slopes of the profiles are not necessarily proportional to the shielding currents, so a hyperbolic profile, for example, does not mean that there is a single direction current circulating parallel to the z-axis! Although these effects are clearly related to the asymmetry and shape of the field in the case of the cylinder, the following physical idea helps to get a further intuitive picture of the differences between the slab and cylinder geometries. The critical state model arises, for the slab, from the equilibrium between the Lorentz-like and the pinning forces, which results in linear flux profiles with slopes proportional to the critical current density, J_c. However, the circular vortices appearing in the cylinder are submitted to a new effect: a "shrinking force" which tends to reduce the vortex radius to zero (this is connected with the corresponding free energy decrease [1,10]). We can think that this force contributes to the rearrangement of the flux in such a way that the magnitudes of the slopes are no longer proportional to J_c, but increase from the outer to the inner walls of the cylinder in such a way that, for example, one can find a slope smaller that J_c close to $r = b$ (small vortex density), while the slope is

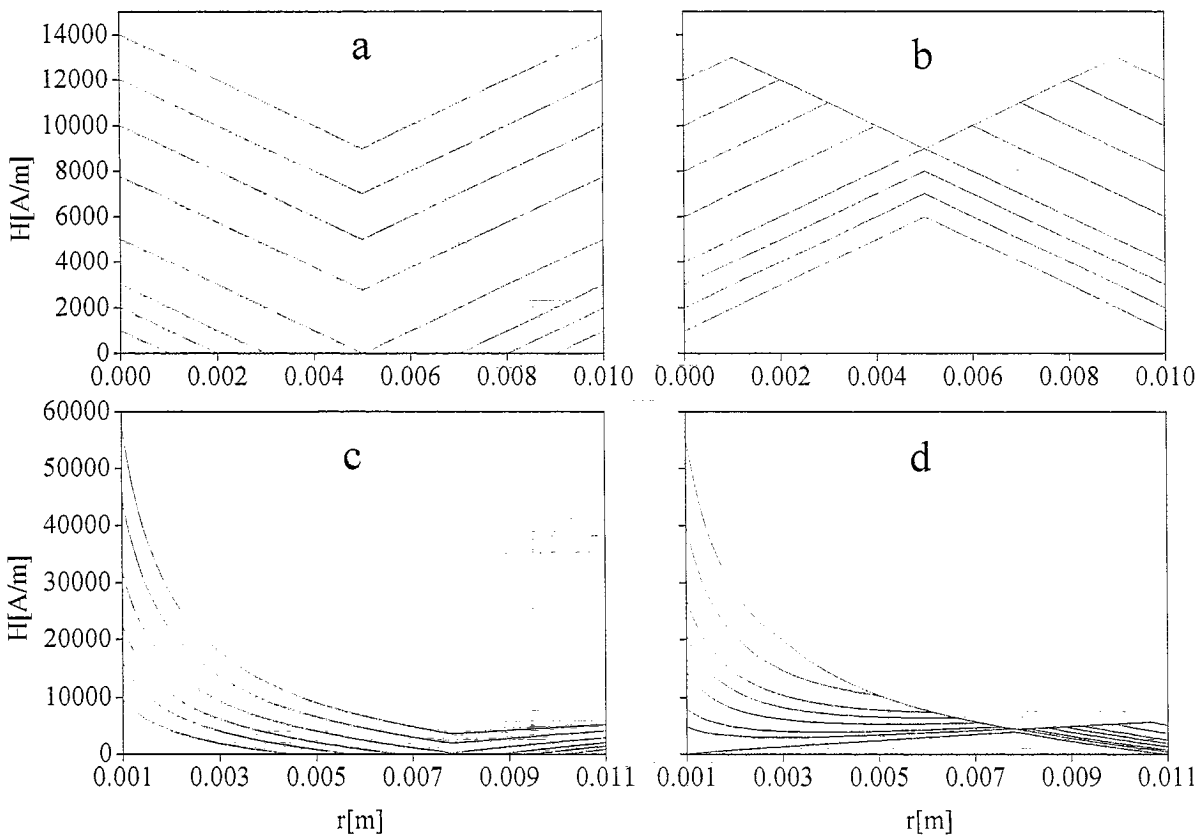

Fig. 3. Flux distribution profiles following Bean's hypothesis. (a) and (b) 10 mm thick infinite slab for increasing and decreasing fields, respectively; (c) and (d) 10 mm thick wall hollow cylinder for increasing and decreasing azimuthal field, respectively. The field in (b) decreases from a maximum of 700 A/m, while it decreases from 6000 A/m in (d).

bigger than J_c close to $r = a$ (high vortex density). This can be quite easily checked out, as a matter of fact, for the profiles depicted in Fig. 3(c).

The magnetization of the hollow cylinder can be calculated, in a straightforward fashion, by substituting the flux distribution expressions, Eqs. (8)–(24), in:

$$M = \frac{B}{\mu_0} - H \tag{25}$$

where

$$B = \frac{\iiint h(r)\,\mathrm{d}v}{\iiint \mathrm{d}v} \tag{26}$$

and

$$H = \frac{\int_a^b \frac{i}{2\pi r}\,\mathrm{d}r}{\int_a^b \mathrm{d}r} = \frac{i}{2\pi(b-a)}\ln\left(\frac{b}{a}\right) \tag{27}$$

In Eq. (26) the integration takes place over the superconducting volume. The average expressed by Eq. (27), however, has been used for H since here the magnetic field is not uniform, as in the case of the slab (note that the integrand of the upper integral is just the magnetic field if there was no superconducting material).

We obtained the following results for the magnetization of the hollow cylinder.

Increasing field

(a) $i < i^*$

$$M = \frac{1}{(b-a)}\left[\frac{i}{4\pi}\ln\left(\frac{\frac{i}{\pi}+J_c a^2}{J_c b^2 - \frac{i}{\pi}}\right) + \frac{J_c a^2}{2}\ln\left(\frac{\sqrt{\frac{1}{J_c}\left(\frac{i}{\pi}+J_c a^2\right)}}{a}\right) + \frac{J_c b^2}{2}\ln\left(\frac{\sqrt{\frac{1}{J_c}\left(J_c b^2 - \frac{i}{\pi}\right)}}{b}\right)\right] \tag{28}$$

(b) $i > i^*$

$$M = \frac{-J_c}{4(b-a)}\left[a^2\ln\left(\frac{a^2+b^2}{2b^2}\right) + b^2\ln\left(\frac{a^2+b^2}{2b^2}\right)\right] \tag{29}$$

Decreasing field

Case (1) $2i^* < i_{max}$

(a) $i_{max} - 2i^* < i < i_{max}$

$$M = \frac{-1}{b-a}\left[\frac{i-i_{max}}{4\pi}\ln\left(\frac{J_c a^2 + \frac{i_{max}-i}{2\pi}}{J_c b^2 - \frac{i_{max}-i}{2\pi}}\right) + \frac{J_c a^2}{2}\ln\left(\frac{a\sqrt{\frac{b^2+a^2}{2}}}{a^2 + \frac{i_{max}-i}{2\pi J_c}}\right) + \frac{J_c b^2}{2}\ln\left(\frac{b\sqrt{\frac{b^2+a^2}{2}}}{b^2 - \frac{i_{max}-i}{2\pi J_c}}\right)\right] \tag{30}$$

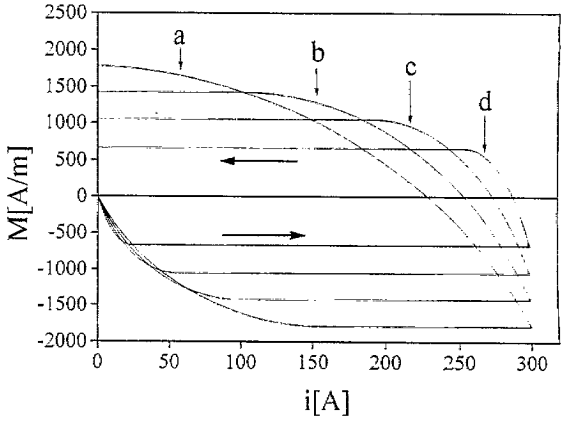

Fig. 4. Dependence of the azimuthal magnetization with the wire current for different wall thicknesses following Bean's hypothesis. (a) $b - a = 10$ mm, (b) $b - a = 7$ mm, (c) $b - a = 5$ mm and (d) $b - a = 3$ mm.

(b) $0 < i < i_{max} - 2i^*$

$$M = \frac{J_c}{4(b-a)}\left[a^2 \ln\left(\frac{a^2+b^2}{2a^2}\right) + b^2 \ln\left(\frac{a^2+b^2}{2a^2}\right)\right] \quad (31)$$

Case (2) $i_{max} < 2i^*$ (formula (30) holds).

Fig. 4 shows these results for different thicknesses of the wall. As in the case of a slab, the magnetization increases with the applied field (or wire current, in the case of the cylinder), and saturates at a certain value $H = H^*_{cyl}$, which corresponds to the magnetic field at the inner wall of the cylinder when the full penetration current has been reached. It should be noticed that we have used the field at the inner surface of the cylinder in the y-axis of the flux profiles in order to make easier the comparison with the slab geometry, while our choice for the x-axis of the magnetization plot was the wire current, since it readily connects our results with a possible experiment (suggested below).

If we plot H^*_{cyl} versus the thickness of the cylinder wall, we obtain the plot shown in Fig. 5, which also displays the thickness dependence of the full penetration field for a slab according to Bean's hypothesis. After quite linear dependences below a thickness of 1 mm, there is a dramatic departure in the behavior of both systems when the wall is thicker. We believe that the obtention of the dependences depicted in Fig. 5, as extracted from magnetization measurements, would be the strongest experimental test to show the differences between the critical state of the two geometries.

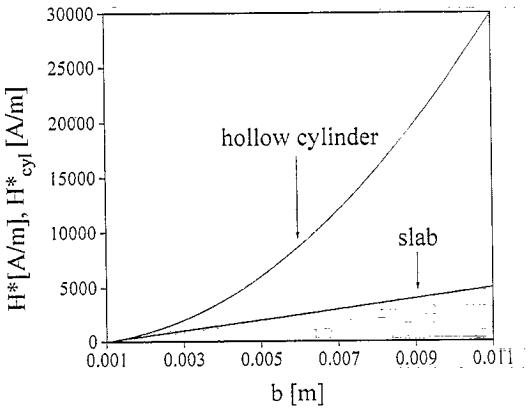

Fig. 5. Dependence of the full penetration field with slab thickness (left surface taken at $r = 1$ mm) and with the thickness of the cylinder wall (inner radius $a = 1$ mm) following Bean's hypothesis.

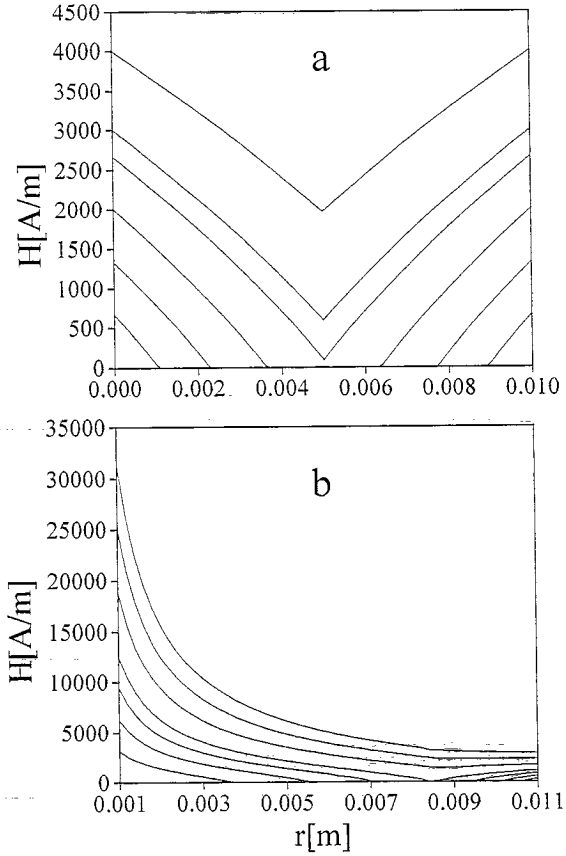

Fig. 6. Flux distribution profiles for increasing fields following Kim's hypothesis. (a) 10 mm thick slab, (b) 10 mm thick wall hollow cylinder.

3.2. Kim's hypothesis

Since Eq. (6), contrary to the case of Bean's hypothesis, does not have an analytical solution, we had to solve it through numerical methods [1]. We computed only the case of increasing wire currents. For the calculations, we used $J_c(0) = 10^6$ A/m^2 ($= 10^2$ A/cm^2) and $h_0/\mu_0 = 700$ A/m (9 Oe). It should be observed that this is around the value of the applied field for which the critical current density

[1] We used the option NDSolve from Mathematica version 2.2 (see Ref. [22]). Additionally, we had to set up a program to deal with the singularity arising when $h = -h_0$.

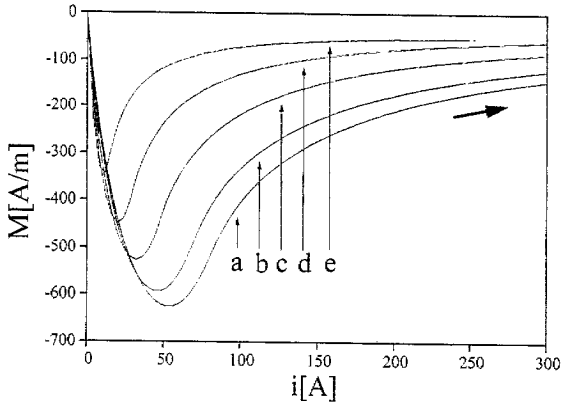

Fig. 7. Dependence of the azimuthal magnetization with the wire current for different cylinder wall thicknesses following Kim's hypothesis. (a) 10 mm, (b) 9 mm, (c) 7 mm, (d) 5 mm and (e) 3 mm.

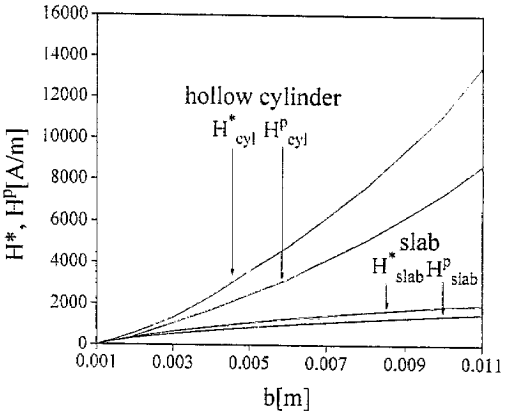

Fig. 8. Dependence of the full penetration field with the thickness of the slab (left surface taken at $r = 1$ mm) and with the thickness of the cylinder wall (inner radius $a = 1$ mm) following Kim's hypothesis. The field at which the magnetization peaks is also plotted against the cylinder wall thickness.

of a typical $YBa_2Cu_3O_7$ ceramic sample decays to half its value at zero field [21]. Fig. 6 shows the flux profiles in the critical state for a 10 mm thick wall hollow cylinder compared with the analogous one corresponding to an infinite slab submitted to a field parallel to its surfaces under Kim's hypothesis. Although both geometries give nonlinear profiles, the curvatures are negative and positive for the slab and the cylinder, respectively. As in the case of Bean's hypothesis, the flux profiles are highly asymmetric for the cylinder. Finally, the hyperbolic-like profiles obtained for relatively high currents should be observed.

Fig. 7 shows the magnetization curves for the cylinder. The maxima typical of the slab geometry (which do not correspond to the respective full penetration currents, as in the case of Bean's hypothesis) are here qualitatively reproduced, as well as the shape of the curves.

Fig. 8 shows the dependence of the full penetration fields and the fields corresponding to the magnetization peaks (H^p_{slab}, H^p_{cyl}), on the thicknesses of the two systems under Kim's hypothesis. Below thicknesses of approximately 1 mm, both characteristics are quite linear, while positive curvature appears in the case of the cylinder for higher thicknesses. A further increase in the dimension of the systems gives greater differences between the slab and cylindrical geometries. If we take into account the strong field dependence of the critical current densities of typical superconducting ceramics with the applied field [21], it is reasonable to believe that an experiment performed on hollow cylinders made of such material could follow our results for Kim's hypothesis. If this is so, "thick" walls must be explored, in order to avoid misleading similarities between the cylindrical and the slab cases occurring for thin walls, as shown in Fig. 8.

A toroidal pick-up coil wound on a superconducting tube would be a good experimental setup for measuring the average azimuthal magnetic induction into the wall, produced by a coaxial current (a similar detection arrangement has been used in Ref. [15] for different purposes in the case of constant geometry superconducting ceramic cylinders). If the current is increased in time at a certain rate, and the coil voltage output is electronically integrated, a signal proportional to the azimuthal magnetic induction will be obtained. The i versus B curves should be measured on cylinders of different outer radii (or on a single cylinder after different reductions of the outer radius by mechanical methods), allowing the attainment of M versus i curves and then, characteristics suitable for comparison with our results as displayed in Figs. 5 and 8. For such an experiment, a very homogeneous superconducting material will be needed in order to avoid the variation of the zero-field

J_c along the radial direction, which would affect the change of the azimuthal magnetization in a misleading way when reducing the outer radius.

4. Conclusions

We have calculated the flux profiles, the magnetization curves, and the thickness dependence of the flux penetration field for the critical state of a superconducting hollow cylinder subject to an azimuthal magnetic field under Bean's and Kim's hypotheses, and compared those characteristics with the "classical" case of a slab submitted to a magnetic field parallel to its surfaces. We obtained detailed analytical expressions for Bean's case and numerical results in Kim's case for the cylindrical geometry considering superconducting parameters similar to those expected for a typical high temperature superconducting ceramic.

The critical state arising from the cylindrical geometry shows some curious differences when compared with the slab one. The cylinder profiles are nonlinear under Bean's hypothesis, while they are linear for the slab geometry. Kim's hypothesis gives nonlinear profiles in both geometries, but the curvatures are opposite. The magnetization curves are qualitatively similar between the slab and the cylinder, but the dependences of the full penetration fields and the fields at which the magnetization peaks show sizable differences for wall thicknesses above a few millimeters. We believe that these latter characteristics are the ideal ones for testing our results experimentally.

Acknowledgements

We would like to thank for fruitful discussions with John Clem, as well as financial support through TWAS grant 92-058 RG/PHYS/LA.

References

[1] M. Tinkham, Introduction to Superconductivity, McGraw-Hill, New York, 1975.
[2] D.R. Nelson, J. Stat. Phys. 57 (1989) 511.
[3] G. Carneiro, Physica C 183 (1991) 360.
[4] P.G. de Gennes, Superconductivity of Metals and Alloys, Benjamin, New York, 1966.
[5] V.A. Kozlov, A.V. Samokhvalov, Pis'ma Zh. Eksp. Teor. Fiz. 53 (1991) 150.
[6] V.A. Kozlov, A.V. Samokhvalov, JETP Lett. 53 (1991) 158.
[7] V.A. Kozlov, A.V. Samokhvalov, Physica C 213 (1993) 103.
[8] Y.A. Genenko, Phys. Rev. B 49 (1994) 6950.
[9] R. Mulet, E. Altshuler, Physica C 252 (1995) 295.
[10] E. Altshuler, R. Mulet, J. Supercond. 8 (1995) 779.
[11] A.V. Samokhvalov, Physica C 259 (1996) 337.
[12] J.R. Clem, Phys. Rev. Lett. 38 (1977) 1425.
[13] M. Shvarster, M. Gitterman, B.Ya. Shapiro, Physica C 264 (1996) 204.
[14] M.A.R. LeBlanc, D. LeBlanc, A. Golebiowski, G. Fillion, Phys. Rev. Lett. 66 (1991) 3309, See, for example.
[15] M.A.R. LeBlanc, S. Celebi, S.X. Wang, V. Plechácêk, Phys. Rev. Lett. 71 (1993) 3367.
[16] C.P. Bean, Phys. Rev. Lett. 8 (1962) 250.
[17] C.P. Bean, Rev. Mod. Phys. (1964) 31.
[18] H. Koppe, Phys. Stat. Sol. 17 (1966) K229.
[19] A. Pérez-González, J.R. Clem, Phys. Rev. B 43 (1991) 7792.
[20] Y.B. Kim, C.F. Hempstead, A.R. Strnad, Phys. Rev. 129 (1962) 528.
[21] E. Altshuler, J. Musa, J. Barroso, A.R.R. Papa, V. Venegas, Cryogenics 33 (1993) 308.
[22] S. Wolframm, Mathematica, Addison-Wesley, Reading, MA, 1993.